(Received 12 July 2025, Accepted 10 September 2025, Scheduled 27 September 2025)

Evaluation of Complex Permittivity for Composite Dispersive Media Including Concrete

Keito Matsuoka, Ryosuke Ozaki*, and Tsuneki Yamasaki

Department of Electrical Engineering, College of Science and Technology, Nihon University, Japan

ABSTRACT: In this paper, the dielectric constant distribution of concrete was determined, which is consistent with the experimental values, and the complex dielectric constants obtained were evaluated. Numerical results are given by resulting complex dielectric constant distributions of four types, the time response waveforms and frequency spectra of a composite dispersive medium consisting of concrete using these dielectric constant distributions, and the time response waveforms and frequency spectra separated by each reflection component. A fast inversion of the Laplace transform method was used for the numerical analysis. Consequently, we were able to clarify the dielectric constant distribution suitable for the analysis by using these time response waveforms and frequency spectra.

1. INTRODUCTION

In recent years, aging and corrosion of buried pipes in addition to buildings (tunnels and roads) constructed during Japan's high economic growth period have become more pronounced, causing road subsidence accidents, burst water pipes, and other serious damage in Japan. Early detection through periodic inspection and maintenance is essential to prevent these accidents, and technologies that enable nondestructive inspection are attracting attention. Ground penetrating radar (GPR) [1, 2] is known to be an effective tool in relatively shallow underground structures under concrete. In general, the electric constants in subsurface media (concrete, soil, and so on) are a function of frequency and need to be treated as a dispersive medium.

In our previous paper [3], we developed a method to determine the unknown coefficients of the complex dielectric constant for fitting to experimental values for soil [4]. The complex dielectric constants are calculated using Sellmeier trinomial with the addition of an orientation polarization term, considering the loss of moisture. We have examined the validity of the obtained complex dielectric constants by using time response analysis.

On the other hand, Refs. [5] and [6] have investigated the electromagnetic field distribution of concrete bridge decks with embedded reinforcing bars using the method of moments (MoM) and the dielectric constant of sub-soil materials such as asphalt, concrete, and soil. In our recent papers [7, 8], the transient scattering problem of the reflection response waveforms has been investigated for the case of a conducting strip buried in the soil medium and that of a multilayered dispersive media structure with the soil of different dielectric constants by using the fast inversion of the Laplace transform (FILT) method [9]. The FILT method can be numerically transformed to the time domain from complex frequency domain. Though we have not investigated the frequency dispersion characteristics of concrete, the papers reported in [5] and [6] analyze the concrete as a lossy medium. In general, the concrete is considered an inhomogeneous medium with a function of space coordinate whose dielectric constant varies with location and depth. Since we can use the FILT method to perform calculations in the complex frequency domain, it is more convenient to treat the medium as having frequency-dependent complex dielectric constants. Accordingly, it is necessary to represent concrete as a dispersive medium as well as soil.

In this paper, the dielectric constant distribution of concrete was determined, which is consistent with the experimental values [10], and complex dielectric constants obtained were evaluated. The evaluation was performed using the following procedures: (1) The time response waveform and frequency spectrum of a single-layer concrete structure were analyzed. (2) The time response waveform and frequency spectrum of a composite dispersive medium consisting of concrete and soil were analyzed. Based on these results, the obtained dielectric constant distributions were evaluated which were suitable for use in the analysis. In addition, the numerical technique for time response waveforms uses the FILT method.

2. SETTING OF PROBLEM

2.1. Analysis Method of Dielectric Constant Distribution

A method is described here for determining the unknown coefficients of the dielectric constant of dispersive media. The dielectric constant of dispersive media $\varepsilon(s)$ is expressed by Sellmeier trinomial and orientational polarization, based on previous paper [3].

$$\frac{\varepsilon(s)}{\varepsilon_0} := 1 + \sum_{L=1}^{3} \frac{\Omega_L^2}{s^2 + g_L s + \gamma_L^2} + \frac{\tau_0}{1 + s\tau}, \quad (1)$$

* Corresponding author: Ryosuke Ozaki (ozaki.ryousuke@nihon-u.ac.jp).

$$= 1 + \frac{\Omega_1^2}{s^2 + g_1 s + \gamma_1^2} + \frac{\Omega_2^2}{s^2 + g_2 s + \gamma_2^2} + \frac{\Omega_3^2}{s^2 + g_3 s + \gamma_3^2} + \frac{\tau_0}{1 + s\tau}, \quad (2)$$

where Ω_L is the plasma frequency; g_L is the loss coefficient; γ_L is the resonance frequency; τ and τ_0 are unknown values for regarding of orientational polarization. $(\Omega_L, g_L, \gamma_L)_{L=1\sim3}$, τ, and τ_0 are unknown coefficients.

Substituting $s = j\omega$ into Eq. (1), the complex dielectric constants are obtained as follows:

$$\left.\frac{\varepsilon(s)}{\varepsilon_0}\right|_{s=j\omega} := \varepsilon_r(\omega) - j\varepsilon_j(\omega), \quad (3)$$

$$\varepsilon_r(\omega) := 1 + \sum_{L=1}^{3} \frac{\Omega_L^2(\gamma_L^2 - \omega^2)}{(\gamma_L^2 - \omega^2)^2 + (\omega g_L)^2} + \frac{\tau_0}{1 + (\omega\tau)^2}, \quad (4)$$

$$\varepsilon_j(\omega) := \frac{\sigma(\omega)}{\omega\varepsilon_0} = \sum_{L=1}^{3} \frac{\Omega_L^2(\omega g_L)}{(\gamma_L^2 - \omega^2)^2 + (\omega g_L)^2} + \frac{\tau_0(\omega\tau)}{1 + (\omega\tau)^2}, \quad (5)$$

where the real and imaginary parts of the complex dielectric constants are defined by Eqs. (4) and (5), respectively. If the eleven unknown coefficients (Ω_1, Ω_2, Ω_3), (g_1, g_2, g_3), (γ_1, γ_2, γ_3), and (τ, τ_0) are determined such that both the real and imaginary parts are simultaneously fitted to the experimental values, the value of complex dielectric constants in Eq. (1) can be obtained.

For the real part, numerator unknown coefficients Ω_1^2, Ω_2^2, Ω_3^2, and τ_0 except $(\gamma_L^2 - \omega^2)$ in Eq. (4) were determined using the following procedure:

First, it is very difficult to determine the eleven unknown coefficients so that both the real and imaginary parts simultaneously fit the experimental values. Therefore, since there are four numerator unknown coefficients Ω_1^2, Ω_2^2, Ω_3^2, and τ_0 in Eq. (4), we expressed a 4×4 matrix equation using these as the unknown values, as shown below:

$$\mathbf{A}_{(l)} \cdot \mathbf{x}_0^{(l)} = \mathbf{B}, \quad (6)$$

where

$$\mathbf{A}_{(l)} := \begin{bmatrix} \frac{(\gamma_1^2-\omega_1^2)}{(\gamma_1^2-\omega_1^2)^2+(\omega_1 g_1)^2} & \frac{(\gamma_2^2-\omega_1^2)}{(\gamma_2^2-\omega_1^2)^2+(\omega_1 g_2)^2} & \frac{(\gamma_3^2-\omega_1^2)}{(\gamma_3^2-\omega_1^2)^2+(\omega_1 g_3)^2} & \frac{1}{1+(\omega_1\tau)^2} \\ \frac{(\gamma_1^2-\omega_2^2)}{(\gamma_1^2-\omega_2^2)^2+(\omega_2 g_1)^2} & \frac{(\gamma_2^2-\omega_2^2)}{(\gamma_2^2-\omega_2^2)^2+(\omega_2 g_2)^2} & \frac{(\gamma_3^2-\omega_2^2)}{(\gamma_3^2-\omega_2^2)^2+(\omega_2 g_3)^2} & \frac{1}{1+(\omega_2\tau)^2} \\ \frac{(\gamma_1^2-\omega_3^2)}{(\gamma_1^2-\omega_3^2)^2+(\omega_3 g_1)^2} & \frac{(\gamma_2^2-\omega_3^2)}{(\gamma_2^2-\omega_3^2)^2+(\omega_3 g_2)^2} & \frac{(\gamma_3^2-\omega_3^2)}{(\gamma_3^2-\omega_3^2)^2+(\omega_3 g_3)^2} & \frac{1}{1+(\omega_3\tau)^2} \\ \frac{(\gamma_1^2-\omega_4^2)}{(\gamma_1^2-\omega_4^2)^2+(\omega_4 g_1)^2} & \frac{(\gamma_2^2-\omega_4^2)}{(\gamma_2^2-\omega_4^2)^2+(\omega_4 g_2)^2} & \frac{(\gamma_3^2-\omega_4^2)}{(\gamma_3^2-\omega_4^2)^2+(\omega_4 g_3)^2} & \frac{1}{1+(\omega_4\tau)^2} \end{bmatrix}$$

$$\mathbf{x}_0^{(l)} := \begin{bmatrix} \Omega_1^2 \\ \Omega_2^2 \\ \Omega_3^2 \\ \tau_0 \end{bmatrix}, \quad \mathbf{B} := \begin{bmatrix} \varepsilon_r(\omega_1) - 1 \\ \varepsilon_r(\omega_2) - 1 \\ \varepsilon_r(\omega_3) - 1 \\ \varepsilon_r(\omega_4) - 1 \end{bmatrix},$$

Matrix $\mathbf{A}_{(l)}$ is the 4×4 square matrix (coefficient matrix); matrix $\mathbf{x}_0^{(l)}$ is the solution vector; matrix $\mathbf{B}$ is the experimental value versus the frequency ω; and variable l indicates the number of computations. By treating the denominator unknown coefficients $(g_L, \gamma_L)_{L=1\sim3}$ and τ as known values and assigning appropriate values to them, the coefficient matrix $\mathbf{A}_{(l)}$ is determined. For matrix $\mathbf{B}$, the experimental values are obtained from literature. Subsequently, four points for the frequency are selected to calculate Eq. (6).

Second, Eqs. (4) and (5) were then calculated for the real and imaginary parts, respectively, using the unknown coefficients $(\Omega_L, g_L, \gamma_L)_{L=1\sim3}$, τ, and τ_0 obtained from the above process.

Next, errors ρ between the two experiments and calculated values were determined by the unknown coefficients obtained from the four points of the real and imaginary parts according to the frequency of matrix $\mathbf{B}$. The error value is set to $|\rho| \leq 10^{-3}$.

Third, if the condition $|\rho| \leq 10^{-3}$ can be satisfied, we verify whether the differential coefficient at the midpoint of the four selected frequency points satisfies the following equation:

$$\frac{d\varepsilon_r(2\pi f_m)}{df} < 0, \quad (7)$$

$$\frac{d\sigma(2\pi f_m)}{df} > 0, \quad (8)$$

If these conditions are not satisfied, the elements of coefficient matrix $\mathbf{A}$ are updated according to the following equation:

$$g_{L,l+1} \leftarrow g_{L,l} + \Delta g, \quad (9)$$

$$\gamma_{L,l+1} \leftarrow \gamma_{L,l} + \Delta\gamma, \quad (10)$$

$$\tau_{l+1} \leftarrow \tau_l + \Delta\tau, \quad (11)$$

The value of Δg, $\Delta\gamma$, $\Delta\tau$ is proportional to the calculation step. Then, the matrix equation in Eq. (6) is solved again, and this process is repeated until the conditions are met.

This method was applied to a concrete medium to determine unknown coefficients of the complex dielectric constant. However, while experimental values for a soil medium are available over a wide frequency range from 30 MHz to 3.84 GHz, the values for a concrete medium are limited to a narrower range from 100 MHz to 1 GHz. Consequently, since the dielectric constant distribution cannot be uniquely determined in the frequency range outside the experimental values, it is necessary to evaluate which dielectric constant distribution is suitable for use in the analysis.

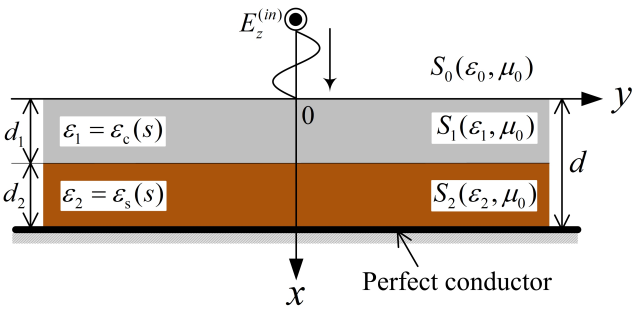

FIGURE 1. Structure and coordinate system of composite dispersive media including concrete.

2.2. Evaluation Based on Time Response Waveforms

Next, the formulation for the reflection coefficient is presented in order to evaluate the obtained dielectric constant distributions based on time response waveforms. The composite dispersive media with concrete embedded with the perfect conductor at $x = d$ is considered, as shown in Fig. 1. The structure in Fig. 1 is uniform in the z-direction. The region $S_0(x < 0)$ represents a dielectric constant ε_0; the regions $S_1(0 \le x < d_1)$ and $S_2(d_1 \le x < d(:= d_1 + d_2))$ are respectfully defined by the dielectric constant ε_1 and ε_2. Here, $\varepsilon_c(s)$ denotes the complex dielectric constant of the concrete medium, and $\varepsilon_s(s)$ represents the complex dielectric constant of the soil medium, which has been investigated in previous paper [3]. The permeability is assumed to be μ_0 in all regions. In this paper, the TE case is discussed (the electric field has only the z-component) for the complex frequency domain in the following formulation.

The electromagnetic fields of regions S_0, S_1, and S_2 are

$$E_z^{(0)}(s,x) = E_z^{(in)}(s,x) + E_z^{(r)}(s,x), \tag{12}$$

$$E_z^{(in)}(s,x) = E_0^{(in)}(s)e^{-k_0(s)x}, \tag{13}$$

$$E_z^{(r)}(s,x) = R(s)e^{k_0(s)x}, \tag{14}$$

$$E_z^{(1)}(s,x) = G_1(s)e^{-k_1(s)x} + G_2(s)e^{k_1(s)x}, \tag{15}$$

$$E_z^{(2)}(s,x) = G_3(s)e^{-k_2(s)x} + G_4(s)e^{k_2(s)x}, \tag{16}$$

$$H_y^{(\alpha)}(s,x) = \frac{1}{s\mu_0}\frac{\partial E_z^{(\alpha)}(s,x)}{\partial x}, \tag{17}$$

$$k_\alpha(s) := s\sqrt{\varepsilon_\alpha\mu_0}\ , \quad (\alpha = 0 \sim 2), \tag{18}$$

where $E_0^{(in)}(s)$ is the image function of the incident sine pulse $E_0^{(in)}(t)$ without a direct current component at $x = 0$, as shown in Fig. 2(a), and its frequency spectrum is shown in Fig. 2(b). Then, $t_w(:= 1/f_0)$ is the pulse width, and f_0 is the center frequency. $k_\alpha(s)$ is the wave number and the propagation constant in the x-direction; $k_0(s)(:= s/c_0)$ is the wave number in free space; c_0 is the velocity of light; and $R(s)$, $G_1(s)$, $G_2(s)$, $G_3(s)$, and $G_4(s)$ are the unknown coefficients to be determined from the boundary conditions.

The equations of boundary conditions are therefore as follows:

$$x = 0 : \begin{cases} E_z^{(0)}(s,x) = E_z^{(1)}(s,x) \\ H_y^{(0)}(s,x) = H_y^{(1)}(s,x) \end{cases}, \tag{19}$$

$$x = d_1 : \begin{cases} E_z^{(1)}(s,x) = E_z^{(2)}(s,x) \\ H_y^{(1)}(s,x) = H_y^{(2)}(s,x) \end{cases}, \tag{20}$$

$$x = d : E_z^{(2)}(s,x) = 0, \tag{21}$$

From the boundary conditions at $x = 0$, $x = d_1$, and $x = d$, the reflection coefficients are obtained as follows:

$$R(s) = \frac{\eta_1(\eta_2 e^{-2k_2(s)d_2} - 1) + (e^{-2k_2(s)d_2} - \eta_2)e^{-2k_1(s)d_1}}{\eta_2 e^{-2k_2(s)d_2} - 1 + \eta_1(e^{-2k_2(s)d_2} - \eta_2)e^{-2k_1(s)d_1}}, \tag{22}$$

where

$$\eta_1 := \frac{1-\Gamma_1}{1+\Gamma_1}, \quad \eta_2 := \frac{1-\Gamma_2/\Gamma_1}{1+\Gamma_2/\Gamma_1},$$

$$\Gamma_1 := \sqrt{\varepsilon_1/\varepsilon_0}, \quad \Gamma_2 := \sqrt{\varepsilon_2/\varepsilon_0}.$$

Here, replacing the numerator and denominator of Eq. (22) with $f_1(s)$ and $f_2(s)$, respectively, the equation is transformed as follows:

$$R(s) = \frac{f_1(s)}{f_2(s)} = f_1(s)\left(f_2(s)\right)^{-1}, \tag{23}$$

The reflection response can be separated by expanding $(f_2(s))^{-1}$ in Eq. (23) and is transformed into a power series. By excluding multiple reflection components, the following expression was obtained:

$$R(s) = \eta_1, \tag{24}$$

$$R(s) = -\eta_2(\eta_1^2 - 1)e^{-2k_1(s)d_1}, \tag{25}$$

$$R(s) = -(\eta_1^2 - 1)(\eta_2^2 - 1)e^{-2k_1(s)d_1 - 2k_2(s)d_2}, \tag{26}$$

Therefore, the reflected electric field $E_z^{(r)}(s,x)$ in the complex frequency domain is obtained by substituting Eq. (22) into Eq. (14). The reflected electric field $E_z^{(r)}(T,X)$ obtained using $R(s)$ was transformed into a normalized time domain using the FILT method [9] with the Euler transformation, as shown in the following equation:

$$E_z^{(r)}(T,X) := \frac{1}{2\pi j}\int_{\beta-j\infty}^{\beta+j\infty} E_z^{(r)}(S,X)e^{ST}dS,$$

$$= \frac{e^a}{T}\left[\sum_{n=1}^{N} F_n + 2^{-J}\sum_{M=1}^{J} C_{JM}F_{N+M}\right], \tag{27}$$

where

$$F_n := (-1)^n \mathrm{Im}\left[E_z^{(r)}(S,X)\right], \quad S := \frac{a + j(n-0.5)\pi}{T},$$

$$C_{JJ} = 1, \quad C_{JM-1} := C_{JM} + \frac{J!}{(M-1)!(J-M+1)!}.$$

where N is the truncation mode number of the FILT method; J is the number of terms in the Euler transformation; a is the approximation parameter; $S(:= st_w)$ is the normalized complex frequency; $T(:= t/t_w)$ is the normalized time; and $X(:= x/(c_0 t_w))$ is the normalized coordinate system.

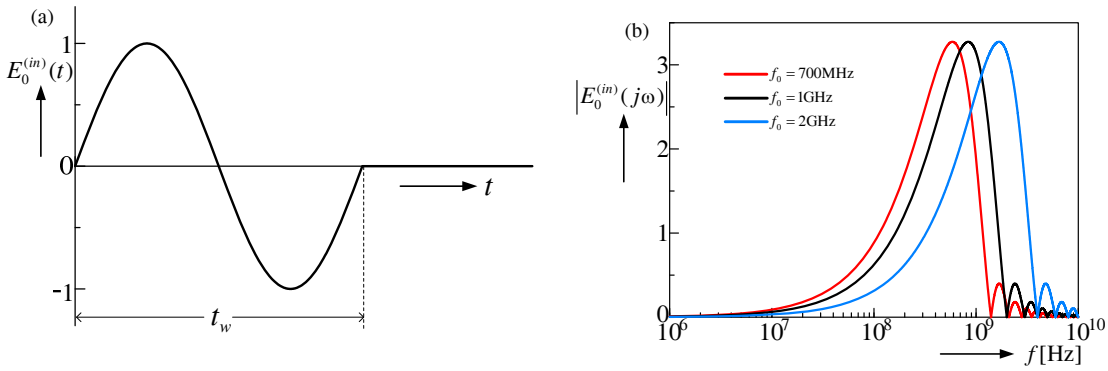

FIGURE 2. Waveform and spectrum of the sine pulse. (a) Waveform. (b) Frequency spectrum.

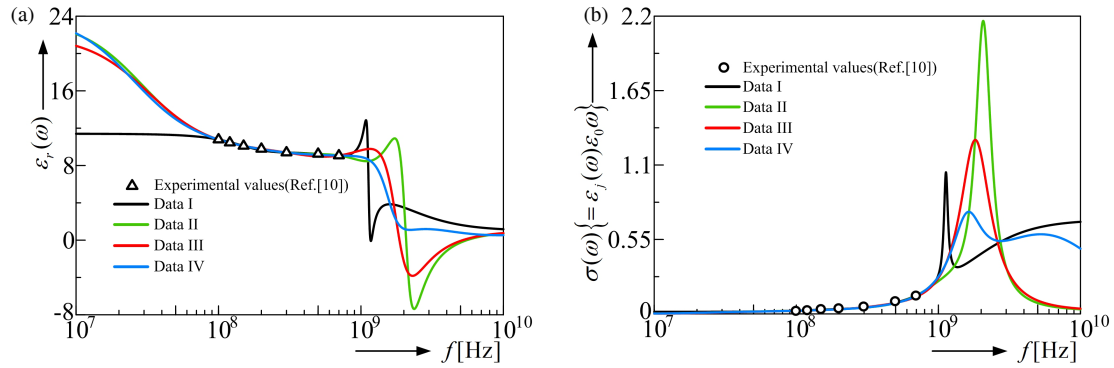

FIGURE 3. Complex dielectric constant distributions of concrete. (a) Real part. (b) Imaginary part.

3. NUMERICAL RESULTS

We performed fitting to the experimental values of concrete. The experimental values are shown in Table 1. When we achieved fitting the complex dielectric constant distribution between the experimental values and calculated values using our past proposed method [3], the two results were in good agreement. Since the frequency range of concrete is included within that of soil, the complex dielectric constant of concrete was expressed using the same Eq. (1) as in [3].

TABLE 1. The experimental values obtained from [10].

f [GHz]	$\varepsilon_r(\omega)$	$\sigma(\omega)\{=\varepsilon_j(\omega)\varepsilon_0\omega\}$
0.10	10.78	0.0190
0.12	10.45	0.0237
0.15	10.10	0.0320
0.20	9.78	0.0378
0.30	9.39	0.0508
0.50	9.24	0.0902
0.70	9.07	0.1318

Based on the experimental values obtained from [10], four sets of the unknown coefficients were determined by performing iterative calculations with our method over about two months. As a result of calculations, the following combinations of values were obtained:

$$\left.\begin{array}{l}\Omega_1 \approx 3.900\times10^9,\ \gamma_1 \approx 1.000\times10^7,\ g_1 \approx 9.000\times10^9\\ \Omega_2 \approx 7.029\times10^9,\ \gamma_2 \approx 7.100\times10^9,\ g_2 \approx 5.500\times10^8\\ \Omega_3 \approx 1.347\times10^9,\ \gamma_3 \approx 1.100\times10^9,\ g_3 \approx 1.570\times10^9\\ \tau_0 \approx 8.109,\ \tau \approx 1.030\times10^{-10}\end{array}\right\} \quad (28)$$

$$\left.\begin{array}{l}\Omega_1 \approx 1.270\times10^9,\ \gamma_1 \approx 1.730\times10^9,\ g_1 \approx 2.555\times10^9\\ \Omega_2 \approx 1.167\times10^{10},\ \gamma_2 \approx 7.100\times10^9,\ g_2 \approx 8.000\times10^9\\ \Omega_3 \approx 3.065\times10^{10},\ \gamma_3 \approx 1.300\times10^{10},\ g_3 \approx 4.000\times10^9\\ \tau_0 \approx 13.76,\ \tau \approx 5.500\times10^{-9}\end{array}\right\} \quad (29)$$

$$\left.\begin{array}{l}\Omega_1 \approx 3.447\times10^9,\ \gamma_1 \approx 3.239\times10^9,\ g_1 \approx 5.085\times10^9\\ \Omega_2 \approx 3.135\times10^{10},\ \gamma_2 \approx 1.143\times10^{10},\ g_2 \approx 6.900\times10^9\\ \Omega_3 \approx 1.204\times10^{10},\ \gamma_3 \approx 1.170\times10^{11},\ g_3 \approx 8.400\times10^9\\ \tau_0 \approx 12.22,\ \tau \approx 4.900\times10^{-9}\end{array}\right\} \quad (30)$$

$$\left.\begin{array}{l}\Omega_1 \approx 1.075\times10^{10},\ \gamma_1 \approx 2.800\times10^9,\ g_1 \approx 4.950\times10^{10}\\ \Omega_2 \approx 7.690\times10^{10},\ \gamma_2 \approx 3.600\times10^{10},\ g_2 \approx 9.600\times10^{10}\\ \Omega_3 \approx 1.852\times10^{10},\ \gamma_3 \approx 1.000\times10^{10},\ g_3 \approx 6.000\times10^9\\ \tau_0 \approx 1.325,\ \tau \approx 9.000\times10^{-10}\end{array}\right\} \quad (31)$$

where Eq. (28) is defined as data I, Eq. (29) as data II, Eq. (30) as data III, and Eq. (31) as data IV. Fig. 3 shows the frequency characteristics obtained by substituting these data into Eqs. (4) and (5). In Fig. 3, the circular (◯) and triangular (△) plots represent experimental values, while the solid lines show the

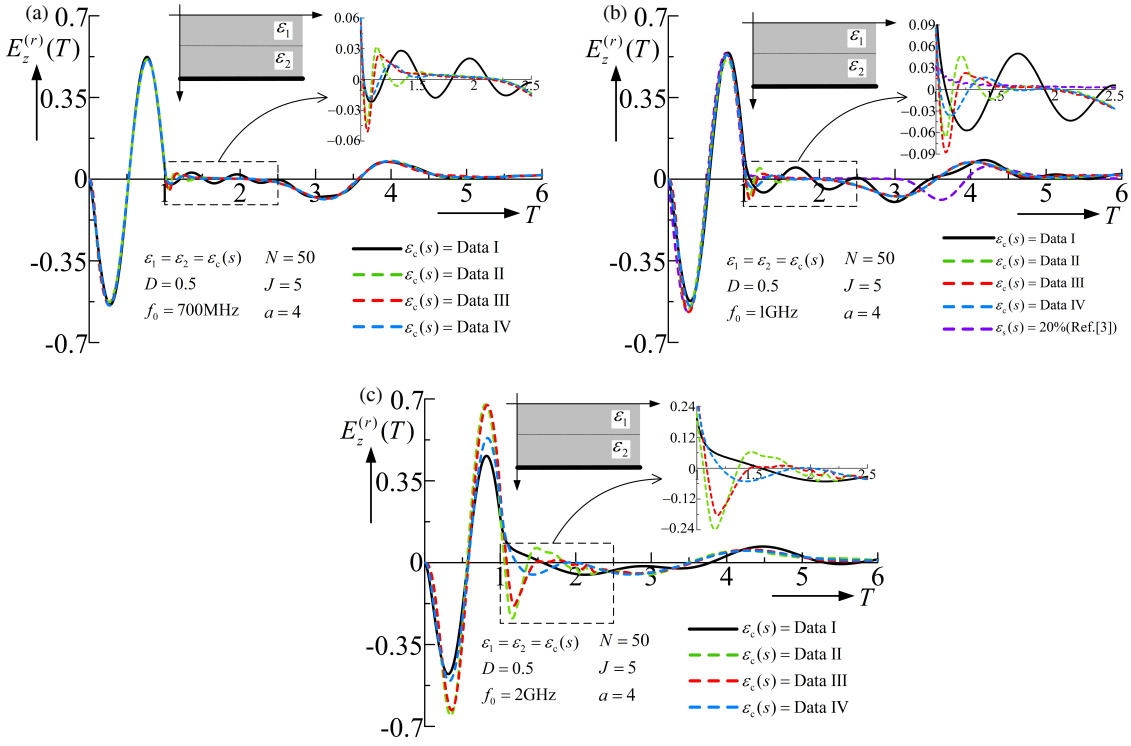

FIGURE 4. Reflection response waveforms with varying data. (a) Case of $f_0 = 700$ MHz. (b) Case of $f_0 = 1$ GHz. (c) Case of $f_0 = 2$ GHz.

results for data I, II, III, and IV, respectively, obtained using the method described in a previous paper [3]. From Fig. 3, the following characteristics can be seen:

(1-1) It can be seen that data I, II, III, and IV show good agreement with the experimental values.

(1-2) When comparing the results of data I, II, III, and IV, it can be seen that the characteristics differ significantly outside certain frequency ranges of the experimental values. The real part shows the differences between the frequency ranges of the $f < 100$ MHz and $f > 1$ GHz, whereas the imaginary part shows differences in the distribution of the $f > 1$ GHz.

(1-3) It can be seen that resonance due to the orientational polarization occurs near $f = 1$ GHz in the real and imaginary parts of data I, II, III, and IV.

To evaluate which of the four obtained data were available, the influence of these data on the time response waveforms was next examined.

The normalized depth $D(:= d/(c_0 t_w)) = 0.5$. The complex dielectric constants were determined as follows: data I, II, III, and IV. For all results, the FILT parameters were fixed at $N = 50$, $J = 5$, $a = 4$.

Figures 4(a), (b), and (c) show the reflection response waveforms obtained with data I, II, III, and IV under the condition of $\varepsilon_1 = \varepsilon_2 = \varepsilon_c(s)$ with varying center frequencies. From these results, the following features f_0 can be observed:

(2-1) From Fig. 4(a), at $T = 1$, the reflection from the surface is observed, and at $T = 2.5$, the reflection from the perfect conductor appears. It can be observed that, in the case of data I, the reflection waveform exhibits oscillations in the range $1 < T < 2.5$, while for data II, III, and IV, undershoot occurs at $T \approx 1$.

(2-2) Figure 4(b) shows that the reflection waveform for the soil medium (with a moisture content of 20%) exhibits neither oscillations nor undershoots/overshoots, in contrast to that for the concrete medium. Therefore, it is assumed that the oscillations and undershoots that occur in the reflection waveform for the concrete medium are caused by the resonance effect near $f = 1$ GHz, resulting from the complex dielectric constant distribution of the concrete.

(2-3) Figure 4(c) shows that the amplitude of the response waveform varies depending on the data. In particular, a significant undershoot can be observed for data II and III.

To investigate the cause of the oscillations and undershoot in the reflection response waveform, the calculation accuracy of the reflection response waveform was confirmed using a convergence test of the truncation mode number $1/N$ in the FILT method, as shown in Fig. 5. Fig. 5 shows the convergence of $E_z^{(r)}(T)$ versus $1/N$ at $T = 1.26$ for data I, II, III, and IV,

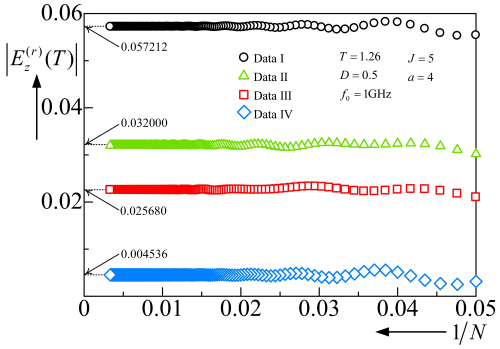

FIGURE 5. Convergence of $|E_z^{(r)}(T)|$ vs. $1/N$.

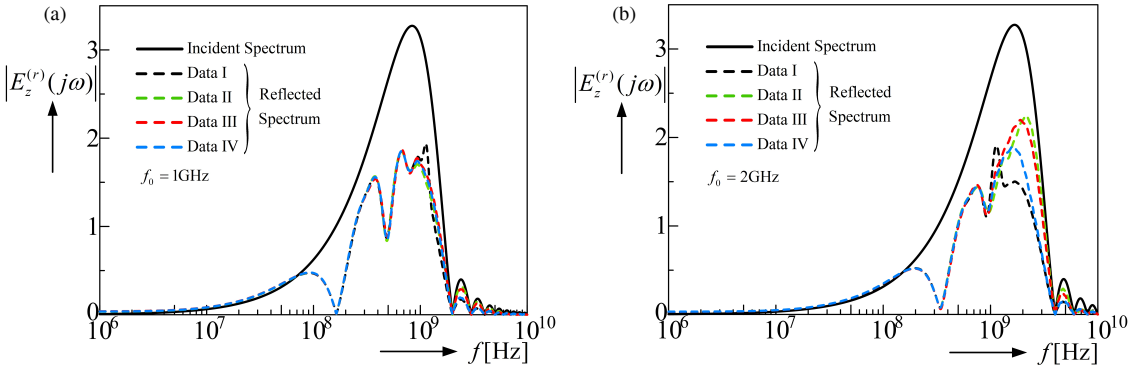

FIGURE 6. Frequency spectrum with varying data. (a) Case of $f_0 = 1$ GHz. (b) Case of $f_0 = 2$ GHz.

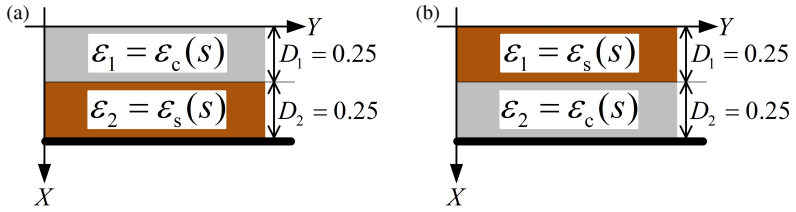

FIGURE 7. Structure to analyze. (a) Structure A. (b) Structure B.

under the same conditions shown in Fig. 4(b). Fig. 5 shows that the relative errors with respect to the extrapolated true values at $N = 50$ are 0.25% for data I, 0.61% for data II, 0.42% for data III, and 0.38% for data IV. Therefore, from the convergence test, we can confirm to obtain the reflection response waveform with high accuracy.

Next, the effect of the complex dielectric constant distribution was investigated based on the frequency spectrum. Figs. 6(a) and (b) show the results obtained by applying the discrete Fourier transform (DFT) of the reflection response waveform in Figs. 4(b) and (c). Fig. 6 shows the following characteristics:

(3-1) Figure 6(a) shows that the amplitude of the reflection spectrum is approximately half that of the incident spectrum. Although slight differences were observed around $f = 1$ GHz, the general characteristics were almost identical.

(3-2) From Fig. 6(b), it can be seen that the reflection spectrum differs in the frequency range of $f = 1$ to 3 GHz. In addition, when the center frequency is higher, the reflection spectrum contains more high-frequency components. Consequently, oscillations and undershoots occur in the reflection response waveform owing to the influence of the resonance that occurs in the high-frequency region of the complex dielectric constant distribution of the concrete medium.

Data I and II led to significant oscillations and undershoots in the reflection response waveform, making them unsuitable for analysis. Therefore, data III and IV were examined in more detail.

Subsequently, the complex dielectric constant distribution of the concrete medium was evaluated using time response waveforms of a composite structure consisting of concrete and soil media with different dispersions.

Structures A and B under investigation are shown in Fig. 7. In both structures, the normalized depths were set to $D_1 = D_2 = 0.25$. Structure A represents the case in which the concrete medium ($\varepsilon_1 = \varepsilon_c(s)$) is placed above the soil medium ($\varepsilon_2 = \varepsilon_s(s)$ with 5% moisture content), whereas structure B represents the case in which the soil medium ($\varepsilon_1 = \varepsilon_s(s)$ with 5% moisture content) is placed above the concrete medium ($\varepsilon_2 = \varepsilon_c(s)$).

Figure 8(a) shows reflection response waveforms of structure A under the same conditions as shown in Fig. 4(b), for data III and IV, respectively. Fig. 8(b) shows reflection response waveforms of structure B under the same conditions as those in Fig. 8(a). The following observations can be derived from Figs. 8(a) and (b):

(6-1) From Fig. 8(a), it can be seen that the reflection from the surface of the concrete medium appears in the range of $0 < T \leq 1$, and the reflection from the perfect conductor appears around $T = 2$. The reflection from the soil medium is barely visible, which is probably because the dielectric constant of the concrete medium is higher than that of the soil medium, resulting in greater transmission. There is also an undershoot at $T = 1$, and its magnitude is smaller for data IV than for data III.

(6-2) From Fig. 8(b), it can be seen that a reflection from the surface of the soil medium occurs in the range $0 < T \leq 1$; a reflection from the concrete medium occurs in the range $1 < T \leq 2$; and a reflection from the perfect conductor occurs around $T = 2$. It can also be observed that the response waveforms for data III and IV are almost identical.

Next, reflection components of each medium in structures A and B were examined using Eqs. (24)–(26), respectively. Figs. 9(a) and 9(b) show time response waveforms of the reflection components from each medium under the same conditions

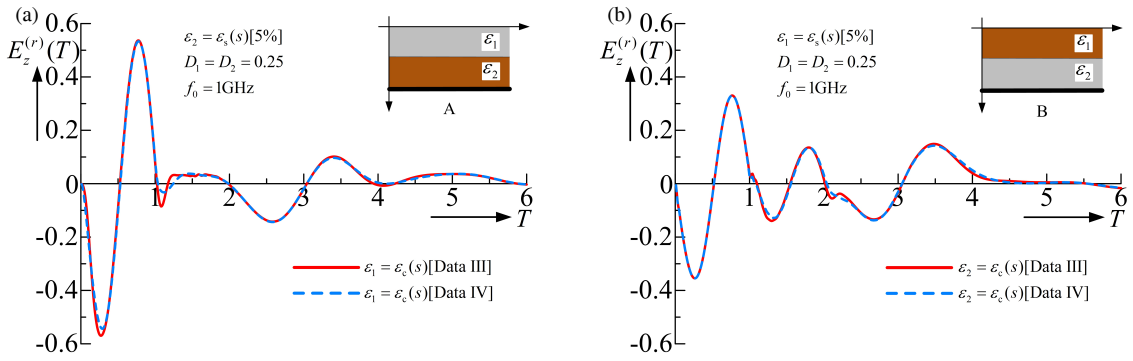

FIGURE 8. Reflection response waveforms with varying center frequencies. (a) Case of structure A. (b) Case of structure B.

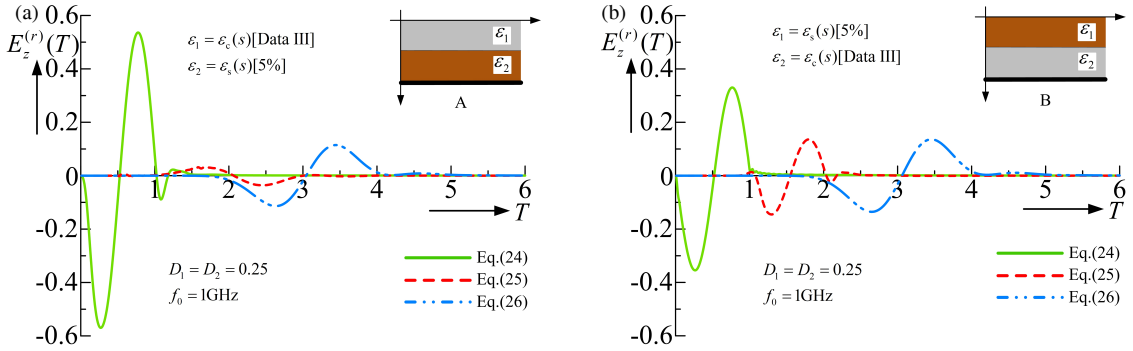

FIGURE 9. Reflection components of each medium (case of data III). (a) Structure A. (b) Structure B.

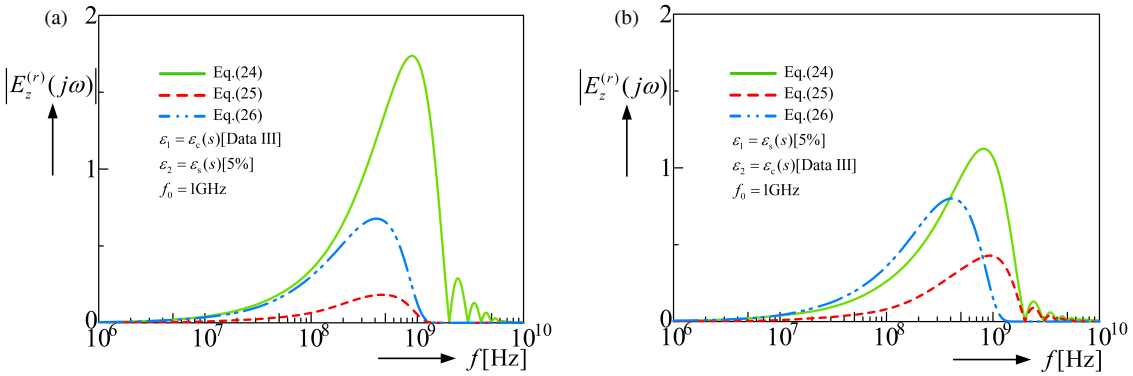

FIGURE 10. Frequency spectrum (case of data III). (a) Structure A. (b) Structure B.

as in Fig. 8, using Eqs. (24)–(26) with data III. From Fig. 9, the following characteristics can be observed:

(7-1) From Fig. 9(a), it can be seen that reflection waves from the surface appear in the range $0 < T \leq 1$, from the soil medium in the range $1 < T \leq 3$, and from the perfect conductor in the range $2 \leq T < 4$. It can also be observed that an undershoot occurs in the surface reflection from the concrete medium.

(7-2) From Fig. 9(b), it can be seen that reflection waves from the surface appear in the range $0 < T \leq 1$, from the concrete medium in the range $1 < T \leq 2$, and from the perfect conductor in the range $2 < T \leq 4$. It can also be observed that an undershoot occurs in the vicinity of $T = 2$ in the reflection from the concrete medium.

Figures 10(a) and (b) show the results of the discrete Fourier transform applied to the reflection response waveforms in Fig. 9. From Fig. 10, it can be seen that the reflection spectrum from the soil medium contains more low-frequency components without including frequencies above the $f = 1$ GHz, whereas the reflection spectrum from the concrete medium contains more high-frequency components, including those above $f = 1$ GHz.

Figures 11(a) and (b) show time response waveforms of the reflection components from each medium using data IV. Fig. 11 shows that an undershoot occurs on part of the reflection response waveform from the concrete medium. Its magnitude is smaller for data IV than for data III.

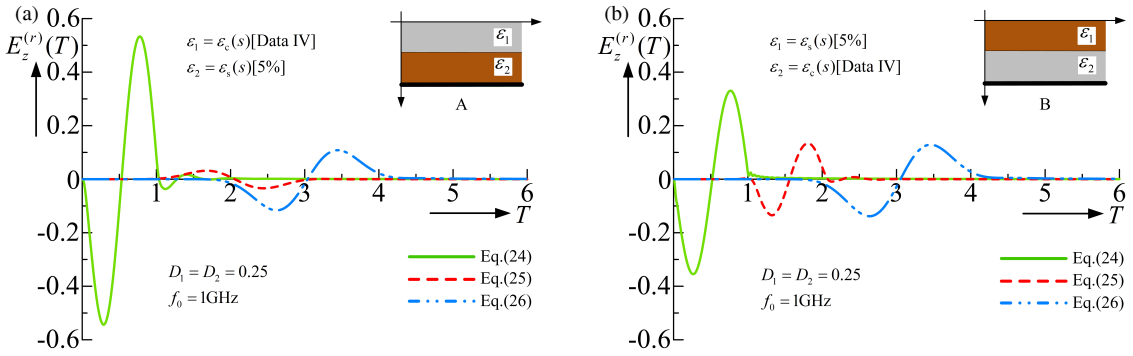

FIGURE 11. Reflection components of each medium (case of data IV). (a) Structure A. (b) Structure B.

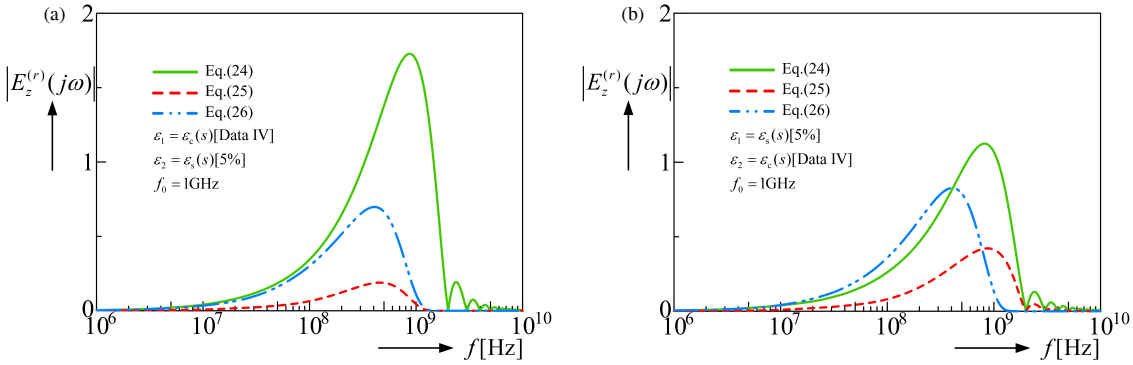

FIGURE 12. Frequency spectrum (case of data IV). (a) Structure A. (b) Structure B.

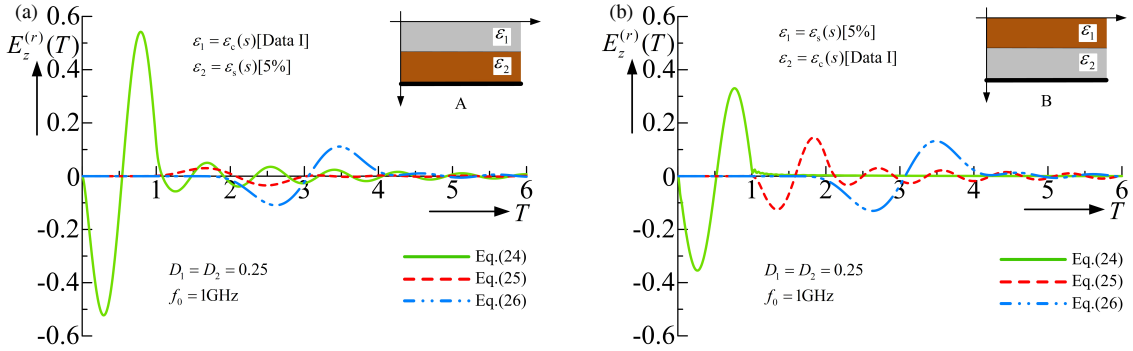

FIGURE 13. Reflection components of each medium (case of data I). (a) Structure A. (b) Structure B.

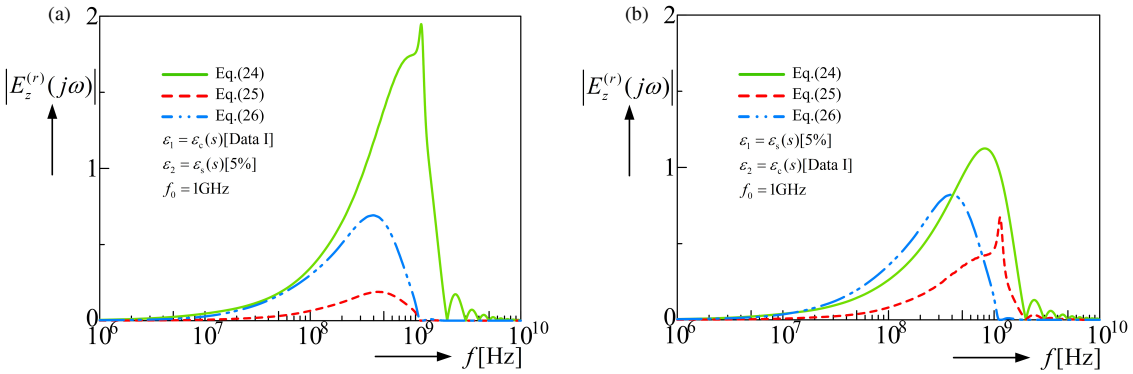

FIGURE 14. Frequency spectrum (case of data I). (a) Structure A. (b) Structure B.

Figures 12(a) and (b) show the results of the discrete Fourier transform applied to the reflection response waveforms in Fig. 11. By comparing Fig. 12 and Fig. 10, it can be seen that their characteristics are almost identical.

Finally, Fig. 13(a) and (b) show time response waveforms of the reflection components from each medium using data I. Fig. 13 shows that the reflection response waveform from the concrete medium exhibits oscillations.

Figures 14(a) and (b) show results of the discrete Fourier transform of reflection response waveforms shown in Fig. 13. Fig. 14 shows that the reflection spectrum from the concrete medium has a peak near $f = 1$ GHz.

Therefore, among the complex dielectric constant data I–IV determined for the concrete medium, data IV of Eq. (31) was considered the most suitable for analysis.

4. CONCLUSIONS

In this paper, a method from a previous paper was applied to a concrete medium to determine the dielectric constant distributions, and the obtained distributions were evaluated. The time response waveforms and frequency spectra of a single-layer concrete structure and a composite dispersive medium consisting of concrete and soil were analyzed to evaluate which dielectric constant distribution was suitable for analysis. It turned out that data IV was the most suitable for the analysis.

In the future, we plan to develop a mathematical model and formulation for reinforced concrete and investigate the reflection response of reinforced concrete structures.

ACKNOWLEDGEMENT

This study was partially supported by the JSPS KAKENHI grant number JP25K07907.

APPENDIX A. DERIVATION OF THE FORMULA OF FILT [14]

The inverse Laplace transform is defined by

$$f(t) = \frac{1}{2\pi j}\int_{\beta-j\infty}^{\beta+j\infty} F(s)e^{st}ds. \tag{A1}$$

FILT is based on the approximation of the exponential function e^{st} in the Bromwich integral. The approximate function $E_{ec}(st, a)$ is represented by

$$\begin{aligned} E_{ec}(st,a) &= \frac{e^a}{2\cosh(a-st)} = e^{st} - e^{-2a}e^{3st} + e^{-4a}e^{5st} - \ldots, \\ &= \frac{e^a}{2}\sum_{n=-\infty}^{\infty} j(-1)^n \frac{1}{st-[a+j(n-0.5)\pi]}, \end{aligned} \tag{A2}$$

where a is the approximate parameter. We replace e^{st} in Eq. (A1) by $E_{ec}(st, a)$. Therefore

$$f(t) := \frac{1}{2\pi j}\int_{\beta-j\infty}^{\beta+j\infty} F(s)E_{ec}(st,a)ds = \frac{e^a}{t}\sum_{n=1}^{\infty} F_n, \tag{A3}$$

where

$$F_n := (-1)^n \mathrm{Im}\left[F\left\{\frac{a+j(n-0.5)\pi}{t}\right\}\right]. \tag{A4}$$

To truncate the infinite series, the Euler transformation is useful for achieving rapid convergence. Considering the transformation, Eq. (A3) can be approximated by

$$f(t) = \frac{e^a}{T}\left[\sum_{n=1}^{N} F_n + 2^{-J}\sum_{M=1}^{J} C_{JM}F_{N+M}\right], \tag{A5}$$

where

$$C_{JJ} = 1, \quad C_{JM-1} := C_{JM} + \frac{J!}{(M-1)!(J-M+1)!},$$

N is the truncation number of FILT, and J is the number of terms in the Euler transformation.

REFERENCES

[1] Persico, R., *Introduction to Ground Penetrating Radar: Inverse Scattering and Data Processing*, John Wiley & Sons, 2014.

[2] Nishimoto, M., K. Nagayoshi, S. Ueno, and Y. Kimura, "Classification of landmine-like objects buried under rough ground surfaces using a ground penetrating radar," *IEICE Transactions on Electronics*, Vol. E90-C, No. 2, 327–333, 2007.

[3] Ozaki, R., N. Sugizaki, and T. Yamasaki, "Numerical analysis of pulse responses in the dispersion media," *IEICE Transactions on Electronics*, Vol. E97-C, No. 1, 45–49, 2014.

[4] Hipp, J. E., "Soil electromagnetic parameters as functions of frequency, soil density, and soil moisture," *Proceedings of the IEEE*, Vol. 62, No. 1, 98–103, 1974.

[5] Tajdini, M. M. and C. M. Rappaport, "Analytic analysis of ground penetrating radar wave scattering of reinforced concrete bridge decks," in *2013 IEEE International Geoscience and Remote Sensing Symposium — IGARSS*, 4066–4069, Melbourne, VIC, Australia, 2013.

[6] Guattari, C., D. Ramaccia, F. Bilotti, and A. Toscano, "Permittivity of sub-soil materials retrieved through transmission line model and GPR data," *Progress In Electromagnetics Research*, Vol. 151, 65–72, 2015.

[7] Ozaki, R., C. Wang, and T. Yamasaki, "Analysis of inside response and electric field distribution by plane grating in dispersive medium," *URSI Radio Science Letters*, Vol. 5, 27, 2024.

[8] Itaya, K., R. Ozaki, and T. Yamasaki, "Fundamental investigation of the transient analysis technique for multilayered dispersive media by filt combined with continued fraction expanded method," *IEICE Transactions on Electronics*, Vol. E107-C, No. 11, 490–493, 2024.

[9] Hosono, T., "Numerical inversion of laplace transform and some applications to wave optics," *Radio Science*, Vol. 16, No. 6, 1015–1019, 1981.

[10] Hosono, T., T. Hinata, and T. Yamasaki, "Prediction of radio wave interference area caused by concrete structures," in *Proc. IEICE General Conf.*, No. 3, 7, 1979 (in Japanese).

[11] Matsuoka, K., R. Ozaki, and T. Yamasaki, "Analysis of complex dielectric constant distribution by concrete medium," in *Proc. IEICE General Conf.*, 2024 (in Japanese).

[12] Matsuoka, K., R. Ozaki, and T. Yamasaki, "Analysis of reflection response for composite media included the concrete," IEICE Tech. Report, 102–107, 2024 (in Japanese).

[13] Matsuoka, K., R. Ozaki, and T. Yamasaki, "Consideration on reflected waveforms extraction for concrete mixed media," in *Proc. IEICE Society Conf. 2024.*, 2024 (in Japanese).

[14] Hosono, T., "International series of monographs on advanced electromagnetic: Filt," *Science House Inc.*, Vol. 2, 2013 (in Japanese).